Vol. 365: 1–16, 2008
doi: 10.3354/meps07610

MARINE ECOLOGY PROGRESS SERIES
Mar Ecol Prog Ser

Published August 18

FEATURE ARTICLE

OPEN ACCESS

Response of Antarctic phytoplankton to solar UVR exposure: inhibition and recovery of photosynthesis in coastal and pelagic assemblages

Jennifer J. Fritz[1,2,*], Patrick J. Neale[1], Richard F. Davis[1,3], Jill A. Peloquin[1,4]

[1]Smithsonian Environmental Research Center, PO Box 28, Edgewater, Maryland 21037, USA

[2]*Present address:* Rosenstiel School of Marine and Atmospheric Sciences/Meteorology and Physical Oceanography, 4600 Rickenbacker Causeway, Miami, Florida 33149, USA

[3]*Present address:* Dept. of Oceanography, Dalhousie University, Halifax, Nova Scotia B3H 4J1, Canada

[4]*Present address:* Institute of Biogeochemistry and Pollutant Dynamics, ETH Zürich, Universitätstr. 16, 8092 Zürich, Switzerland

ABSTRACT: We examined ultraviolet radiation (UVR)-induced inhibition and recovery of Antarctic phytoplankton photosynthesis during the austral spring in surface coastal waters near Palmer Stn and in the open ocean waters of the Weddell-Scotia Confluence from 1997 to 1999. Primary productivity was measured in 12 h time-course experiments using enclosures that transmitted either full-spectrum solar UVR or only long-wavelength UVA. Recovery from inhibition was determined by transferring samples from high to low UVR at intervals during the incubation. Biological weighting functions for UVR inhibition of photosynthesis were also determined for each experiment. Photosynthesis measurements were compared to model predictions using 3 exposure–response relationships: an irradiance-based (*E*) model that assumes rapid repair, a cumulative-exposure (*H*) model that assumes no repair, and a model that incorporated slow repair (*R* model). Open-ocean phytoplankton were generally much more sensitive to UVR inhibition than coastal assemblages, which primarily had high rates of repair (*E* model). In contrast, open-ocean assemblages generally recovered from inhibition more slowly (*R* model). Some recovery was evident in all cases, so the *H* model was not applied to any assemblage. Our previous view of repair being either simply present or absent is therefore revised to recognize that repair rates range from slow to fast and should be taken into account, together with spectral weight, in assessments of photosynthetic response to UVR in the Southern Ocean, including the effect of ozone depletion. Information on repair rate is particularly important for simulations of production in vertically mixed surface layers.

KEY WORDS: Ultraviolet radiation · UVA · UVB · Inhibition of photosynthesis · Biological weighting functions · Polar phytoplankton

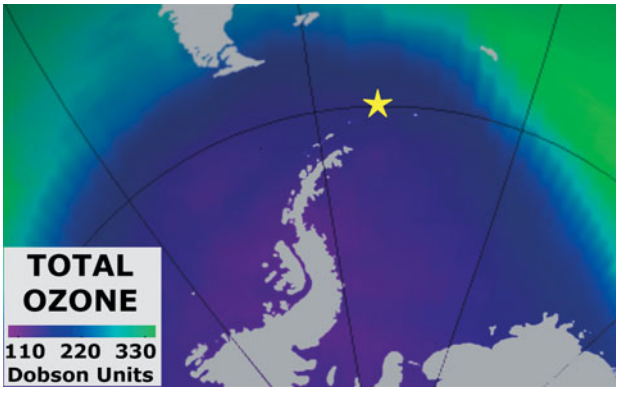

Ozone depletion over the Antarctic Peninsula and adjacent areas on October 20, 1998. Star: location of ARSV 'Laurence M. Gould'.

Photo: NASA Ozone Hole Watch

INTRODUCTION

Solar ultraviolet radiation (UVR, 290 to 400 nm) affects planktonic processes in the surface layer of diverse aquatic environments and, in particular, the metabolism and survival of bacterioplankton, phytoplankton and zooplankton. A subject of much recent work has been the extent to which these effects are augmented by enhanced UVB (290 to 320 nm) due to Antarctic ozone depletion, which is most severe within the springtime polar vortex. This depletion is a consequence of previous anthropogenic release of halocarbons into the atmosphere, which persist in causing effects despite controls instituted by the Montreal Pro-

*Email: jfritz@rsmas.miami.edu

tocol (UNEP 2006). Indeed, ozone depletion during austral spring 2006 was the most severe on record (see NASA press release available at www.sciencedaily.com/releases/2006/10/061019162053.htm#). A special focus has been given to the effects of these variations in UVR on phytoplankton photosynthesis in the Southern Ocean as evidenced by the inclusion of 6 chapters on the topic in an edited book on UVR in Antarctica (Weiler & Penhale 1994). Those studies and numerous others have shown that photosynthesis in the Southern Ocean is inhibited by ambient and enhanced UVR and a continuing challenge is translating such responses into estimates of the effect on productivity in the water column (reviewed in Davidson 2006).

Biological weighting functions (BWFs) quantify the effectiveness (or 'weight') of UVR at causing some biological effect in relation to wavelength (see Cullen & Neale 1997, Neale 2000). They allow the comparison of biological responses to different spectral regions of UVR and can be utilized to predict photosynthetic response to a changing UVR environment when coupled to an appropriate photosynthesis–irradiance (BWF/*P*–*E*) model. Results to date have shown more than 10-fold variation in the sensitivity of phytoplankton photosynthesis to UVR as measured by BWFs, which translates to decreases of 16 to 30% in estimates of the daily primary productivity of lakes, estuaries and Antarctic waters (Neale et al. 1998a,b 2001, Neale 2001, Hiriart-Baer & Smith 2004, Litchman & Neale 2005).

In order to estimate primary productivity, the BWF/*P*–*E* model must take into account not only the spectral irradiance but also the kinetics of inhibition and recovery (Cullen & Lesser 1991, Neale 2000). The time course of inhibition under UVR plus photosynthetically available radiation (PAR) exposure and recovery under PAR can be followed using ^{14}C incorporation or pulse amplitude-modulated (PAM) fluorometry and used to infer UVR damage and repair rates (Neale et al. 1998a, Heraud & Beardall 2000, Litchman et al. 2002, Hiriart-Baer & Smith 2004, 2005, Sobrino et al. 2005). For a wide range of phytoplankton cultures and natural assemblages, responses are consistent with repair being proportional to UVR damage, so that the photosynthetic rate rapidly attains an irradiance-dependent steady state (i.e. repair balances damage) (Litchman et al. 2002, Shelly et al. 2003, Litchman & Neale 2005, Sobrino et al. 2005). In this context, repair refers to any process that restores lost photosynthetic capacity, including turnover of membrane complexes and enzymes (further discussion in Vincent & Neale 2000). In contrast, kinetic studies with phytoplankton from the Weddell-Scotia Confluence (WSC) found negligible recovery after strongly inhibitory UVR exposure (Neale et al. 1998a), so that response was best modeled as a function of cumulative radiant exposure. Two exposure response models have been used to predict photosynthesis under these limiting cases of irradiance (*E* model) or cumulative radiant exposure (*H* model) dependence (Neale 2000).

More recently, neither the *E* nor *H* models were found to be satisfactory predictors of the spectral and temporal variations of UVR inhibition and recovery of photosynthesis in phytoplankton assemblages in Lake Erie (Hiriart-Baer & Smith 2004). Estimated damage and, particularly, repair rates were sufficiently slow such that steady state was not attained even over exposures of hours. In this case a more general exposure response model (*R* model) was required in which UVR-dependent damage and repair rates are explicitly defined. The *E* and *H* models are actually special cases of the *R* model under the assumption of steady state or no repair, respectively (Neale 2000). The choice of response model significantly affects the prediction of integrated effects over the water column especially with the inclusion of simulated vertical mixing in the surface layer (Neale et al. 2003, Hiriart-Baer & Smith 2005).

Despite the critical importance of kinetic responses to modeling UVR effects in vertically mixed surface layers, there are few observations of the temporal responses of Southern Ocean phytoplankton assemblages. Although Neale et al. (1998a) reported no significant recovery of photosynthesis after UVR inhibition of WSC assemblages, they cautioned that this was after strongly inhibitory treatment and the response to milder treatments needed to be measured. Moreover, it is unknown whether the WSC assemblages are representative of other Southern Ocean phytoplankton. Here, we report on an extensive set of observations of the UVR responses of phytoplankton assemblages in the WSC and coastal waters of the Western Antarctic Peninsula. UVR responses were measured using both spectral (laboratory incubator) and temporal (incubations using ambient UVR) approaches. The results are examined in terms of the applicability of the *E* model, the *H* model and a version of the *R* model.

MATERIALS AND METHODS

Sampling station details. We sampled the peninsular region of Antarctica during the austral spring season (Fig. 1). In 1997 and 1999, seawater was collected from the coastal waters in the immediate vicinity of Palmer Stn (PAL), Antarctica, near the Long-Term Ecological Research (LTER) Stns A, B and E. During October and November 1998, seawater was collected on a cruise aboard the ARSV 'Laurence M. Gould' in the WSC. Station details are given in Table 1. Four of the WSC stations were from the open ocean and Stn WSC-04 was in the

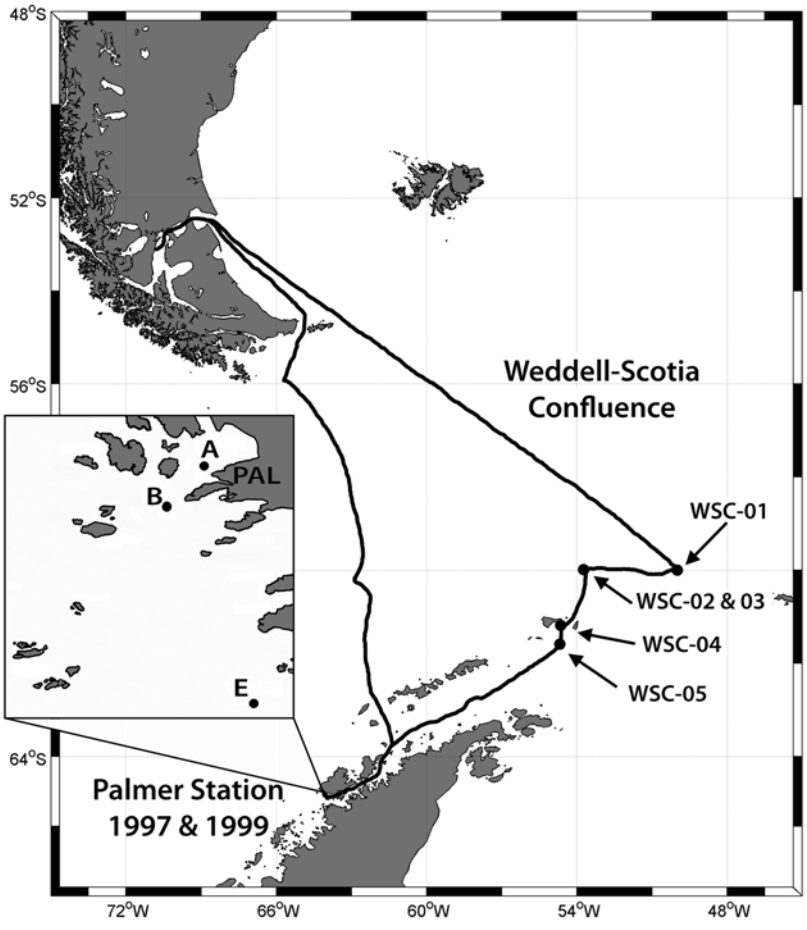

Fig. 1. Locations for the Weddell-Scotia Confluence (WSC) cruise track and Palmer Station (PAL). Inset map of waters near PAL shows the locations of Long-Term Ecological Research (LTER) A, B and E sampling stations. Actual locations are described in Table 1

coastal waters near Elephant Island (Fig. 1). For the WSC, we used the ship's CTD-rosette (20 l Niskin bottles) for these samples and at PAL, we used a 5 l Niskin bottle for samples at depth or a clean bucket for retrieving surface water. Pack ice, when present, was gently moved aside prior to sampling. On 2 occasions when algae were abundant in localized patches of seawater/ice slurries on the surface of pack ice (Stns PAL-06 and PAL-08), the slurry was sampled with a clean bucket. Liquid seawater with suspended algae was strained from the mixture and used immediately for measurements. All samples were collected in the early morning, at least 4 h before local solar noon.

UVR and PAR measurements. UVB and short-wavelength UVA (320 to 400 nm) was measured using the Smithsonian Institution SR-18 scanning UVB radiometer (Neale et al. 2005). This instrument has seventeen 2 nm bandwidth filters ranging from 290 to 322 nm and an additional 10 nm bandwidth 330 nm filter. The radiometer scans 14 times min^{-1} and provides 1 min averages. At PAL, the instrument was located on top of a building located 150 m uphill from the main station and in the WSC, it was mounted on a platform at the top of the ship's mast.

Table 1. Sampling information for the Weddell-Scotia Confluence (WSC) and Palmer (PAL) stations, with corresponding Long-Term Ecological Research (LTER) station name in superscript. DU, Dobson Units. UVR index is from the SR-18 radiometer. Z_{SL}, surface layer depth. K_{dPAR}, attenuation coefficient for photosynthetically available radiation (PAR). nd, not determined. ne, not estimated because water column was stratified (Stns WSC-04 and PAL-11) or because the sample was a surface ice-slurry (Stns PAL-06 and PAL-08). All other samples were taken in open water

Stn	Date	Location	Depth (m)	Chl (mg m^{-3})	Ozone (DU)	UVR index	Z_{SL} (m)	K_{dPAR} (m^{-1})
WSC-01	20 Oct 98	60.00° S, 50.00° W	16	3.5	157	3.2	100	0.142
WSC-02	26 Oct 98	60.00° S, 53.73° W	14	7.9	338	1.6	50	0.205
WSC-03	29 Oct 98	60.00° S, 53.42° W	15	7.4	376	1.4	65	0.188
WSC-04	04 Nov 98	61.19° S, 54.63° W	32	0.4	377	1.8	ne	0.041
WSC-05	07 Nov 98	61.59° S, 54.67° W	33	3.1	223	4.9	70	0.121
PAL-01^{A}	26 Nov 97	64.77° S, 64.05° W	13	1.5	336	4.3	13	0.085
PAL-02^{E}	06 Dec 97	64.82° S, 64.04° W	0	0.4	300	5.5	3.5	0.117
PAL-03^{A}	24 Oct 99	64.77° S, 64.05° W	0	1.8	178	5.2	nd	nd
PAL-04^{E}	30 Oct 99	64.82° S, 64.04° W	0	0.9	245	2.7	nd	nd
PAL-05^{A}	04 Nov 99	64.77° S, 64.05° W	0	1.1	340	2.3	nd	nd
PAL-06^{A}	08 Nov 99	64.77° S, 64.05° W	0	22.5	320	1.0	ne	nd
PAL-07^{B}	11 Nov 99	64.78° S, 64.07° W	0	0.7	222	3.0	2	0.101
PAL-08^{A}	15 Nov 99	64.77° S, 64.05° W	0	31.8	357	2.5	ne	nd
PAL-09^{B}	20 Nov 99	64.78° S, 64.07° W	5	0.8	231	3.2	6	0.102
PAL-10^{A}	22 Nov 99	64.77° S, 64.05° W	0	0.6	290	1.8	6	0.102
PAL-11^{E}	01 Dec 99	64.82° S, 64.04° W	5	1.6	330	3.5	ne	0.151

The UV index, a measure of midday UVR, was calculated by applying the McKinlay & Diffey (1987) BWF for sunburn to each spectrum obtained during the 1 h surrounding solar noon. The weighted irradiance (mW m^{-2}) was subsequently integrated across the spectrum, divided by 25, and averaged over the hour in accordance with the National Weather Service definition of the UV index.

UVA spectral irradiances for PAL were provided by a Biospherical Instruments (BSI) SUV-100 high-resolution scanning UVR radiometer. This unit was installed in the same building as the SR-18 with the light collector located at the top of the building and co-planar with the SR-18 light collector. PAR (W m^{-2}, 400 to 700 nm) was estimated as 50% of total incident irradiance (280 to 2800 nm) measured by an Eppley Laboratory PSP pyranometer. In the WSC, UVA irradiance spectra were obtained using the STAR radiative transfer model. The procedure is described in detail in Neale et al. (2005). In brief, clear sky spectra, 290 to 700 nm, were calculated using observed geographic position, atmospheric pressure and total column ozone from TOMS (available at http://toms.gsfc.nasa.gov). The ratio between SR-18 observations and the STAR clear-sky calculation at 320 nm was applied as a cloudiness correction. SUV measurements and STAR calculations were performed at 15 min intervals, and spectra were estimated at 1 min intervals by adjusting time-interpolated spectra to match the SR-18 at 320 nm. PAR was determined using either the Satlantic multichannel visible detection system (MVDS), which measures spectral irradiance (μW cm^{-2} nm^{-1}) in 7 wavebands between 325 and 700 nm, or the STAR model. An average of the visible channels of the MVDS was calculated and converted to E_{PAR} in W m^{-2} based on a separate correlation with the PAR channel of a BSI GUV-511C radiometer. As a second check, we compared the MVDS-estimated E_{PAR} to the STAR-estimated E_{PAR}.

Attenuation coefficients for PAR (K_{dPAR}) were estimated by log-linear regression on depth profiles of E_{PAR} measured with a BSI PUV-500 radiometer. The depth of the surface layer (Z_{SL}) was estimated from concurrently measured temperature profiles. Sample light history was calculated as a mean percentage of surface PAR irradiance for the surface layer where $\%E_0 = (1 - e^{-K_{dPAR} \cdot Z_{SL}}) \times (K_{dPAR} \cdot Z_{SL})^{-1} \times 100$, or at the sampling depth when the surface layer was stratified where $\%E_0 = e^{-K_{dPAR} \cdot Z_{SL}} \times 100$.

Enclosure description. Time-course incubations were conducted under solar exposure in enclosures that transmitted the full UVR spectrum (high UVR) or excluded all but the longest wavelength UVA (low UVR) (Fig. 2). In 1997, enclosures were constructed from Rohm & Haas Plexiglas (UF-3 for low UVR; UVT for high UVR), whereas in 1998 and 1999, enclosures were made from Rohm & Haas Plexiglas G and Acrylite OP4 for low and high UVR, respectively. Levels of PAR were the same between the high and low UVR conditions. Enclosures were covered with mesh screens that reduced incubation irradiance to 40–50% of incident irradiance. Scalar (4π) PAR irradiance in the enclosures was measured using a BSI QSL-100 quantum irradiance meter with a spherical Teflon light collector. Irradiance measurements included attenuation due to the enclosure as well as the incubation bottles described in the next paragraph.

Productivity measurements. Uptake of carbon into total organic compounds was measured using ^{14}C-sodium bicarbonate. The radioisotope was added to the samples early in the day when UVR was low and total activity was measured to confirm the isotope addition. Incubations were started at approximately 09:30 h local time and lasted for 9 to 12 h. Subsamples were taken every 2.5 to 3 h. Water samples were incubated in triplicate 250 ml Teflon (Nalgene FEP) bottles that are transparent to all wavelengths of solar UVR. Bottles were acid-cleaned and extensively rinsed with ultrapure water and sample water before use. To study recovery, 12 bottles were incubated in a sequence of exposures of high UVR (H) and low UVR (L) throughout the total incubation period (Table 2). Each bottle was identified as HxLy, where x and y are the number of time blocks that the bottle was in the H and L enclosures, respectively. H4 remained in the high UVR enclosure and L4 remained in the low UVR enclosure for the entire incubation (typically 4 time blocks). H1L3

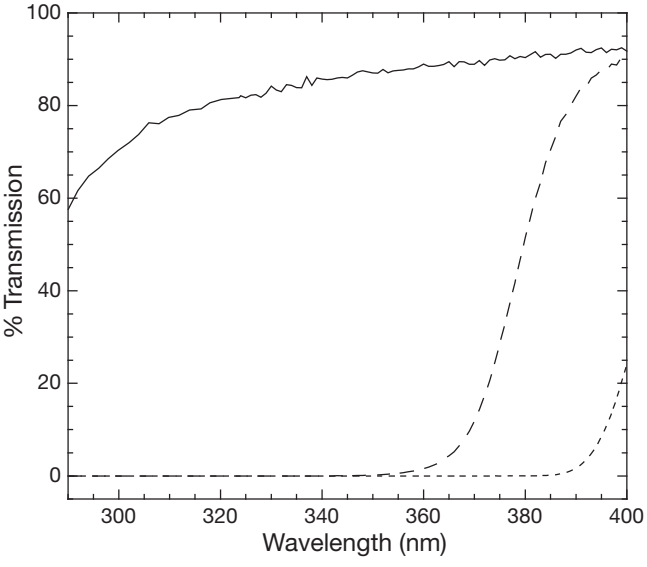

Fig. 2. Percent spectral transmission of enclosures used for full-spectrum UVR exposure (high UVR, ———) and enclosures with only long-wavelength UVA (low UVR: 1997 data, - - - - - - ; 1998 and 1999 data, — — —). This includes transmission through the acrylic tank and the Teflon bottle

Table 2. Incubation scenarios for the 4 types of UVR exposure during the 4 time blocks. L and H signify that the bottles were in the low-UVR and high-UVR enclosures, respectively. Bottles H1L3 and H2L2 were moved from high to low UVR at intermediate times in the incubation (e.g. H1L3: 1 time block at high UVR, 3 time blocks at low UVR)

Elapsed time of incubation (h)	Exposure scenario			
	L4	H1L3	H2L2	H4
2.5	L	H	H	H
5	L	L	H	H
7.5	L	L	L	H
10	L	L	L	H

was in the H enclosure for 1 time block, then moved to the L enclosure for the remainder of the incubation. H2L2 was in the H enclosure for 2 time blocks before being moved to the L enclosure. Two additional bottles were placed in dark bags that excluded UVR and PAR for the entire incubation to determine dark uptake. Subsampling consisted of transferring duplicate or triplicate 10 ml aliquots from each bottle into 20 ml scintillation vials. Hydrochloric acid was added to a final concentration of 0.5% to stop the incubation. Samples were placed on a shaker table in the hood for at least 12 h then evaporated to 3 ml in an oven. Ecolume cocktail was added to each vial and samples were read on a scintillation counter.

Samples without added ^{14}C were incubated in 2 l Teflon bottles in high (H4) and low (L4) UVR conditions and subsampled for measurement of dissolved inorganic carbon and chlorophyll at each time point. Dissolved inorganic carbon was estimated from the total alkalinity, which was measured on duplicate filtered seawater samples according to Parsons et al. (1984). Chlorophyll concentration was determined fluorometrically. Triplicate aliquots of both the initial and subsamples were filtered onto Whatman GF/F filters, extracted in 90% acetone for at least 24 h at –20°C and measured before and after acidification on a calibrated Turner Designs model 10-005 fluorometer.

Average photosynthetic rate was calculated by subtracting the time zero from the post-incubation activity, multiplying by the dissolved inorganic carbon, and dividing by the total radioactivity per sample and the length of time of the incubation. Data were then corrected for the rate of dark uptake and normalized to chlorophyll concentration to give units of mg C (mg chl)$^{-1}$ h^{-1}.

Predicted productivity. Three photoinhibition models (termed *E*, *H* and *R*) were used to examine irradiance and time-dependent photosynthesis. The first was the steady-state, irradiance model (*E* model; Cullen et al. 1992):

$$P^B = P^B_{pot}\left(\frac{1}{1+E^*_{inh}}\right) \quad (1)$$

where P^B_{pot} is the potential photosynthetic rate in the absence of UVR ($P^B_{pot} = P^B_s[1 - e^{-(E_{PAR}/E_s)}]$), P^B is biomass-normalized photosynthesis, P^B_s is the light-saturated rate of photosynthesis in the absence of inhibition, E_{PAR} is PAR and E_s is a characteristic irradiance for light saturation (both in W m^{-2}). E^*_{inh} (non-dimensional) is inhibitory irradiance including both UVR and PAR defined as:

$$E^*_{inh} = \sum_{\lambda=280}^{700} E(\lambda)\cdot\varepsilon_E(\lambda)\cdot\Delta\lambda \quad (2)$$

where $\varepsilon_E(\lambda)$ (reciprocal mW m^{-2}) are the BWF weightings that quantify effectiveness of spectral exposure, $E(\lambda)$ (mW m^{-2} nm^{-1}). In the second model examined, the cumulative-exposure model (*H* model; Neale et al. 1998a) in which repair is negligible, there is an exposure-dependent decrease of photosynthesis from an initial rate:

$$P^B_t = P^B_0\cdot e^{-H^*_{inh}} \quad (3)$$

and average photosynthesis during an exposure period is:

$$P^B = P^B_{pot}\left(\frac{1-e^{-H^*_{inh}}}{H^*_{inh}}\right) \quad (4)$$

where H^*_{inh} (non-dimensional) is inhibitory exposure:

$$H^*_{inh} = \sum_{\lambda=280}^{700} H(\lambda)\cdot\varepsilon_H(\lambda)\cdot\Delta\lambda \quad (5)$$

$H(\lambda) = \int_0^T E(\lambda)\cdot dt$ is radiant exposure (J m^{-2} nm^{-1}) over time period *T*, and $\varepsilon_H(\lambda)$ are the weightings that quantify the effects of radiant exposure (reciprocal J m^{-2}).

Hiriart-Baer & Smith (2004) introduced the *R* model to describe damage and repair kinetics in photosynthesis. This model is useful when neither the *E* nor the *H* model is appropriate due to a low, but significant, level of repair. Like Hiriart-Baer & Smith (2004), we accounted for damage and repair over discrete time intervals of exposure (1 min) using the equation:

$$\frac{dP^*_t}{dt} = -k\cdot P^*_t + r(1-P^*_t) \quad (6)$$

where $P^*_t = P^B_t/P^B_{pot}$ is the relative photosynthesis at time *t* during the incubation, *k* is damage rate and *r* is repair rate (both min^{-1}). Photosynthesis during an incubation was calculated by numerical approximation using the time-step equation $P^*_{t+1} = P^*_t + \frac{dP^*_t}{dt}\Delta t$, which by substitution with Eq. (6) yields:

$$P^*_{t+1} = P^*_t(1-H^*_{inh-t}) + r\Delta t(1-P^*_t) \quad (7)$$

where H^*_{inh-t} is inhibitory exposure over Δt = 1 min time-step using the *R* model BWF, $\varepsilon_R(\lambda)$ (reciprocal J m^{-2}), i.e. $H^*_{inh-t} = 0.06\cdot\left(\sum_{\lambda=280}^{700} E(\lambda)\cdot\varepsilon_R(\lambda)\cdot\Delta\lambda\right)\Delta t$. The

scaling factor, 0.06, is required when $E(\lambda)$ is in mW m^{-2} nm^{-1}.

Predicted photosynthesis was calculated from the UVR measurements described above ('UVR and PAR measurements') and BWFs, P_s^B and E_s parameters estimated from BWF experiments conducted on the same day. Spectral irradiance was adjusted for transmission of the tank, Teflon bottle and mesh screens. For simplicity, inhibition by PAR was represented by the product of E_{PAR} and average PAR weight, ε_{PAR} (reciprocal W m^{-2}). BWFs were determined as described in Neale et al. (2001), in which photosynthesis as a function of PAR and UVR was measured from uptake of ^{14}C-sodium bicarbonate during 1 h exposures in a specially designed spectral incubator, the 'photoinhibitron'. As previously described by Neale & Fritz (2001), this incubator has 80 different irradiance treatments with larger volumes (5 to 10 ml) than were possible in a previous version (Cullen et al. 1992, Neale et al. 1994). Spectral treatments were defined by Schott glass long-pass filters that excluded irradiance for wavelengths shorter than 8 different cutoff (nominal 50% T) wavelengths between 280 and 400 nm. A 2.5 kW Xe arc lamp illuminated the samples, neutral density screening was used to vary the intensity, and a circulating water bath maintained temperature at –1.0 ± 1°C. Spectral irradiance for each treatment in the incubator was measured using a custom-built spectroradiometer with a fiber-optic collector (Neale & Fritz 2001).

BWFs were first estimated using the *H* or *E* model, based on initial kinetic observations of cumulative exposure dependence in the WSC (Neale et al. 1998a) and irradiance dependence at PAL (Neale et al. 2001). Non-linear regression was performed using the principal component analysis (PAL) or Rundel (WSC) methods, as described by Cullen & Neale (1997). The Rundel approach was necessary for the WSC data because of larger variability associated with shipboard operations in rough seas. Photosynthesis was then predicted for the irradiance conditions of the time-course incubations. When the *E* or *H* model failed to provide an acceptable prediction (see 'Results'), the *R* model was fitted. The equation for average rate in the photoinhibitron incubation (cf. Eq. 2 in Hiriart-Baer & Smith 2004) is:

$$P^B = P^B_{pot}\left(\underbrace{\frac{H^*_{inh}\left[1-e^{-(H^*_{inh}+rT)}\right]}{(H^*_{inh}+rT)^2}}_{time\text{-}dependent} + \underbrace{\frac{rT}{H^*_{inh}+rT}}_{steady\text{-}state}\right) \quad (8)$$

where *T* is incubation time (60 min). The first 2 models are simplified cases of the *R* model, i.e. the *H* model is the time-dependent term with $r = 0$ and the *E* model is the steady-state term. An iterative approach was used to estimate repair rate, *r*. Initially, a BWF was fitted to photoinhibitron data with $r = 0$ (equivalent to *H* model); the $\varepsilon_R(\lambda)$ were used to estimate photosynthesis time-courses based on spectral irradiance in each treatment (Eq. 7) with *r* adjusted (by Excel Solver) to obtain best agreement with measured rates by minimizing the sum of squared errors (SSE) between predicted and measured average rate over all time blocks (n = 16 for all except Stn WSC-01 where n = 12). The *R*-model BWF was then re-fitted using this new *r* in Eq. (8). The procedure was repeated until it converged on an estimate of *r* (relative change in $r < 10^{-3}$). The SE of *r* was estimated based on the limits for a 5% increase in SSE.

RESULTS

Hydrography and irradiance

Aside from the surface ice slurry samples, the highest chlorophyll concentrations were found in the open ocean stations of the WSC (Table 1). These stations had surface mixed layers exceeding 50 m and high PAR attenuation, similar to conditions found by Neale et al. (1998b). Chlorophyll in coastal samples (PAL and Stn WSC-04) was <1.8 mg chl m^{-3}. These stations had either a shallow surface mixed layer or stratification at the sample depth. Ozone concentrations during the incubations ranged from 157 to 376 Dobson Units (DU) with 7 sampling days where ozone was <300 DU. UV index ranged from 1.0 to 5.5 with the highest indices (>5.0) at PAL in 1997 and 1999, indicating greater UVR present during the midday hours on those days (Table 1). Given the shallower surface mixed layers and sampling depths at PAL, the light history experienced by populations ($\%E_0$) and the mean daily PAR ($\overline{E}_{PAR}$) within the enclosures on the sampling day were also somewhat higher for the PAL stations (Table 3).

Productivity

Photosynthesis in time-course incubations was consistently higher in the low UVR (L4) tank than in the high UVR (H4) tank. In some cases L4 samples were not significantly different than H4 due to high sample variability primarily within the latter half of the incubation. The *E* model was appropriate for most PAL stations with high R^2 and predicted values within 1 SE of the measurements (Table 3, Fig. 3). However, the observed H4 values for Stn PAL-11 were significantly lower, at less than half of the *E* model predictions, and were subsequently better fit using the *R* model (see next paragraph). Weighted irradiance (E^*_{inh}) was highest in the first 3 incubation blocks (Fig. 3, right *y*-axes), with peak values generally between 16:00 and 18:00 h

Table 3. Photosynthetic parameters for all stations. P^B_s, maximum photosynthetic rate. E_s, light saturation parameter. $\%E_0$, sample light history as mean percent of surface photosynthetically available radiation (PAR) for the surface layer or at sample depth when stratified. $\overline{E}_{PAR}$, mean PAR irradiance during the time-course experiments. The weight from the biological weighting function (BWF) at 320 nm is given for the *E* model ($\varepsilon_E(320)$) or the *R* model ($\varepsilon_R(320)$) (see 'Predicted productivity'). RMSe, overall root mean square error, i.e. the difference between observed and predicted rates in the time-course incubation. nd, not determined. ne, not estimated because the sample was a surface ice-slurry (Stns PAL-06 and PAL-08)

Stn	P^B_s (mg C [mg chl]$^{-1}$ h^{-1})	E_s (W m^{-2})	$\%E_0$	$\overline{E}_{PAR}$ (W m^{-2})	R^2	$\varepsilon_E(320)$ $\times 10^{-4}$ ([mW m^{-2}]$^{-1}$)	$\varepsilon_R(320)$ $\times 10^{-4}$ ([J m^{-2}]$^{-1}$)	Repair $\times 10^{-3}$ (min^{-1})	RMSe (mg C [mg chl]$^{-1}$ h^{-1})
WSC-01	3.25 ± 0.24	21.7	7.1	52	0.87		0.67	10.98	0.29
WS-02	2.80 ± 0.13	21.2	9.7	86	0.91		0.84	8.00	0.20
WSC-03	2.74 ± 0.17	20.5	8.2	69	0.86		0.82	6.84	0.31
WSC-04	2.39 ± 0.57	25.9	26.6	61	0.80	8.10			0.36
WSC-05	3.35 ± 0.24	17.7	11.8	69	0.85		0.36	6.99	0.32
PAL-01	1.48 ± 0.12	21.5	33.1	106	0.90	1.83			0.55
PAL-02	2.59 ± 0.20	14.0	66.4	138	0.88	0.78			0.44
PAL-03	1.31 ± 0.10	21.5	nd	90	0.91	0.96			0.42
PAL-04	1.88 ± 0.13	16.2	nd	46	0.88	1.24			0.44
PAL-05	1.55 ± 0.10	12.1	nd	67	0.92	2.34			0.52
PAL-06	1.43 ± 0.08	25.8	ne	43	0.94	0.86			0.21
PAL-07	2.30 ± 0.21	19.3	90.5	65	0.90	1.97			0.63
PAL-08	1.63 ± 0.11	29.4	ne	101	0.94	0.68			0.19
PAL-09	1.71 ± 0.12	17.0	74.8	70	0.91	1.36			0.24
PAL-10	1.84 ± 0.17	22.2	74.8	47	0.89	1.44			0.21
PAL-11	1.07 ± 0.07	18.5	47.0	100	0.92		0.68	8.01	0.11

GMT, except Stn PAL-10 (Fig. 3D), which was a stormy day with $E^*_{inh} < 0.6$ for the whole day.

Previous work suggested that the *H* model would be applicable to WSC assemblages as opposed to the *E* model (Neale et al. 1998a). When we fitted an *H* model to photoinhibitron measurements and predicted time courses for the H4 incubation, these agreed for the first time block but predicted activity was very low to negligible afterwards due to a complete lack of repair (Fig. 4). This was in sharp contrast to observed H4 time courses, in which significant productivity remained through the exposure period (Fig. 4), indicating that there was some level of ongoing repair. On the other hand, the *E* model did not reproduce all features of the time course, particularly partial recovery after high to low UVR transfer (data not shown). Prediction of intermediate rates of recovery required application of the *R* model (Hiriart-Baer & Smith 2004). The *R* model provided good agreement between the measured and predicted photosynthesis for 4 WSC stations and also for Stn PAL-11 (Fig. 5). The repair rate of Stn WSC-04 from the coastal waters near Elephant Island was too high to be resolved by our experimental approach (iterative estimate of *r* did not converge); however, an acceptable fit was obtained with the *E* model (Table 3). This station was more similar to PAL stations in its shallow surface layer depth, low K_{dPAR} and higher average PAR exposure than the other open-ocean assemblages (Tables 1 & 3).

Considering all stations, predicted photosynthesis generally agreed with observed measurements for H4 and L4 (Fig. 6) with most points within 1 SE of a 1:1 relationship for both PAL (n = 88) and WSC (n = 38). The slope of predicted versus observed photosynthesis, estimated by linear regression through the origin, was not significantly different from 1 for the *R* model fits (0.97, SE = 0.03, n = 38). The slope for the *E* model fits was <1 (0.91, SE = 0.03, n = 88), indicating a slight tendency to underestimate photosynthesis. Overall model skill measured by the correlation between measured and observed was higher for the *R* model (0.87) compared to the *E* model (0.50). In part this is due to the extra parameter in the *R* model that was fitted using the time series data, whereas *E* model predictions were independent from the time series data. Predicted photosynthesis also agreed well with measured rates for transferred samples, as discussed in the 'Repair rate' subsection.

Model input

Parameters generated from BWF analysis and used to predict time-course measurements are given in Table 3. The fit of the photoinhibitron data to the BWF/*P*–*E* model was good with R^2 values of 0.85 or better (n = 70 to 80 experiment^{-1}). In general, open-ocean samples had higher maximum chlorophyll-specific photosynthetic rates compared to coastal samples. Rates in the WSC ranged from 2.39 to 3.25 mg C (mg chl)$^{-1}$ h^{-1}, whereas rates at PAL were from 1.07 to 2.59 mg C (mg chl)$^{-1}$ h^{-1}, with only 2 locations with

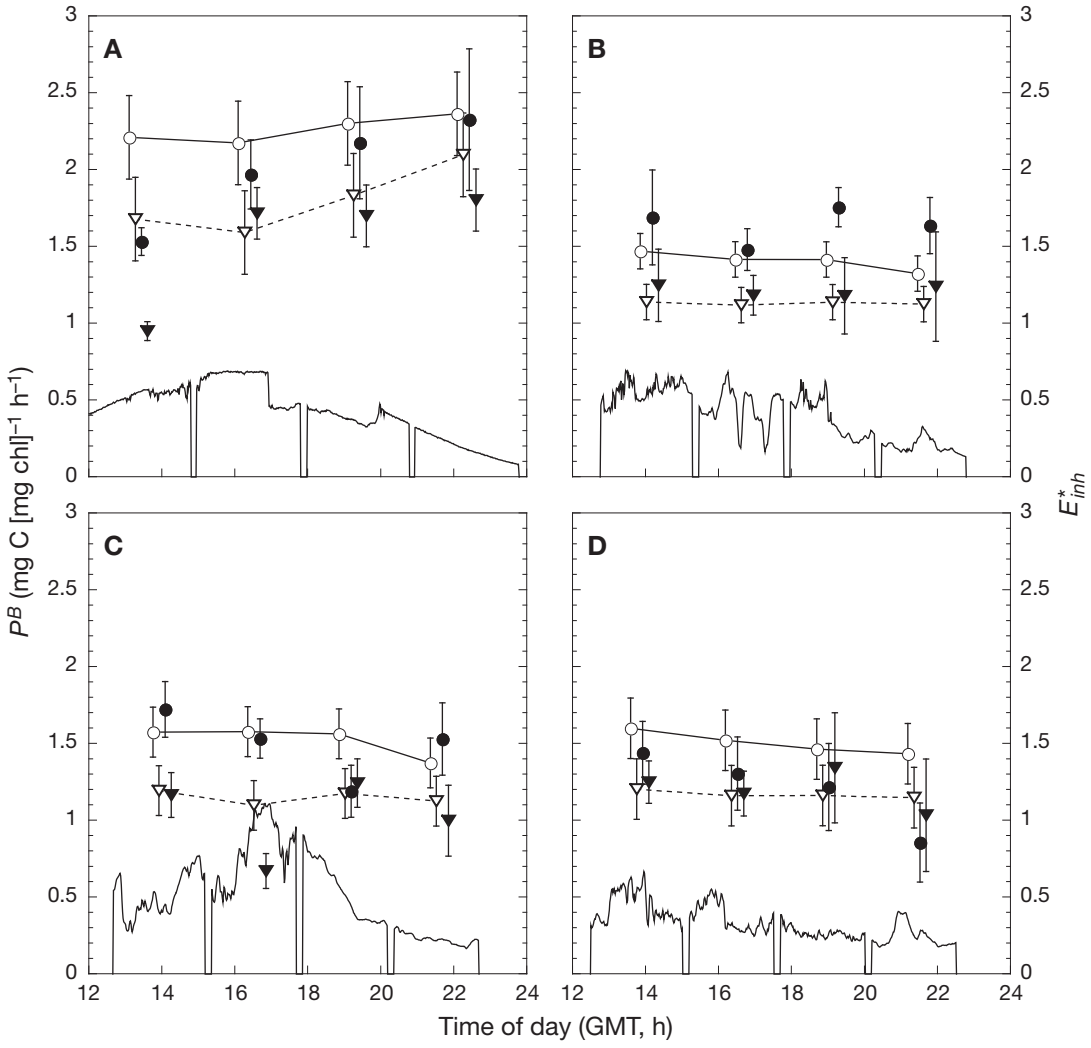

Fig. 3. Average photosynthesis using the *E* model (see 'Predicted productivity') for Stns (A) PAL-02, (B) PAL-08, (C) PAL-09 and (D) PAL-10 in 1997 and 1999. Predicted data include L4 (—○—) and H4 (- - -▽- - -). Observed data include L4 (●) and H4 (▼) (see Table 2). Weighted UVR ($E^{\star}_{inh}$) in the high-UVR tank is the solid line in the lower portion and uses the right *y*-axis on each plot. Error bars denote SE of measurements or of *E* model predictions

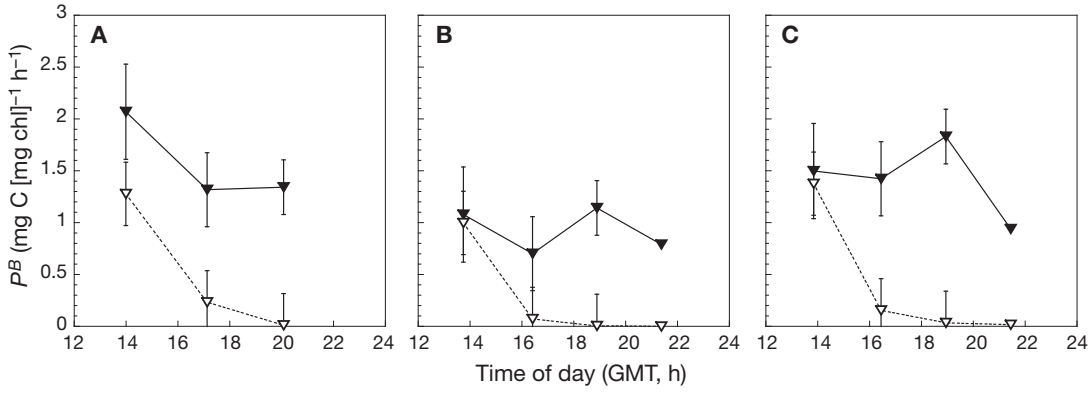

Fig. 4. Observed (—▼—) and predicted (- - -▽- - -) photosynthesis for 3 WSC populations exposed to high UVR (H4) using the cumulative exposure model without repair included. Stns (A) WSC-01, (B) WSC-02 and (C) WSC-05. Error bars denote SE of measurements or of *H* model predictions

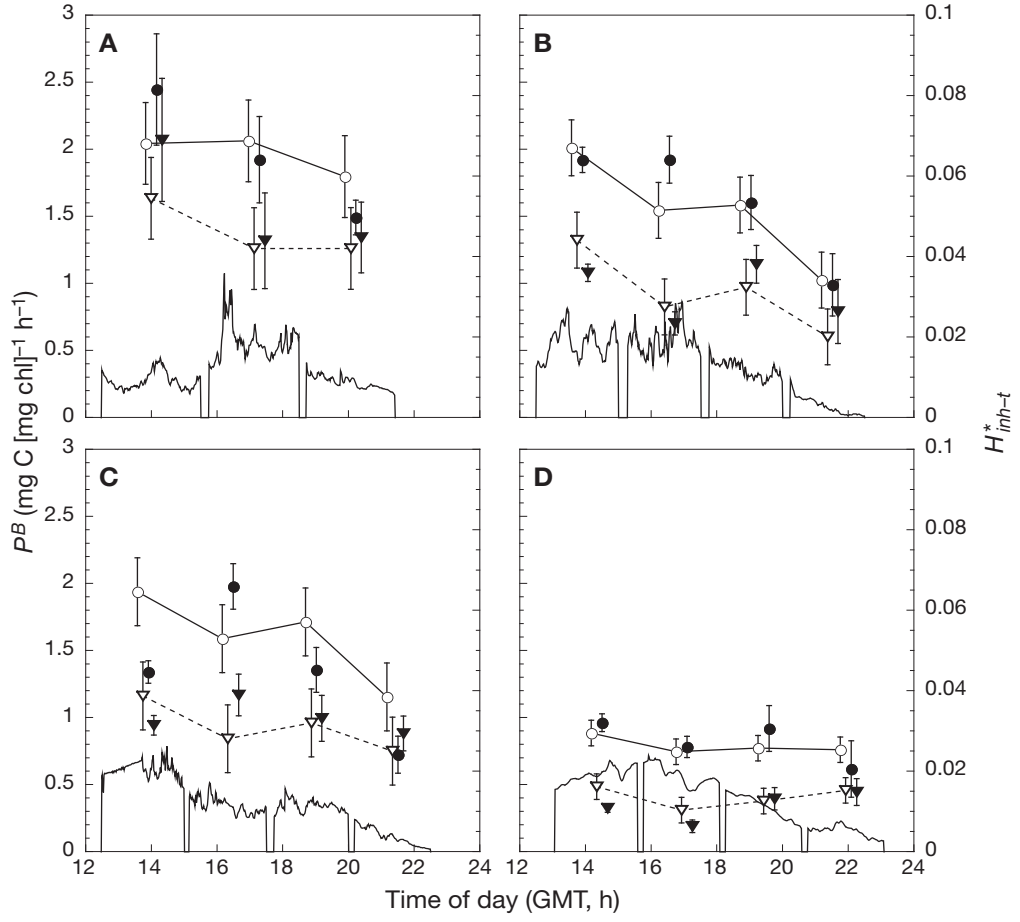

Fig. 5. Average photosynthesis for *R* model (see 'Predicted productivity') populations at Stns (A) WSC-01, (B) WSC-02, (C) WSC-03 and (D) PAL-11. Predicted data include: L4 (—○—) and H4 (- - -▽- - -). Observed data include: L4 (●) and H4 (▼) (see Table 2). Weighted UVR over 1 min time intervals (H^*_{inh-t}) in the high-UVR tank is the solid line in the lower portion and uses the right *y*-axis on each plot. Error bars denote SE of measurements or of *R* model predictions

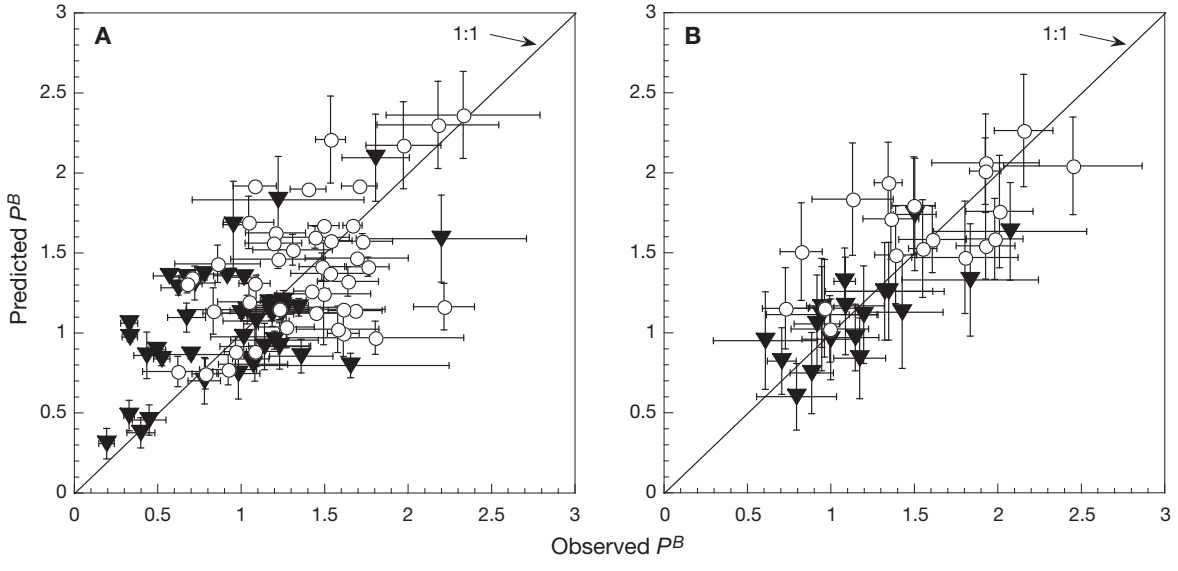

Fig. 6. Predicted versus observed photosynthesis using the applicable *E* or *R* model for all stations at (A) PAL in 1997 and 1999 and (B) WSC in 1998. Samples from L4 (○) and samples from H4 (▼). Vertical bars are SE for model predictions. Horizontal bars are SE of measurements

rates >2.0. The inhibition weight at 320 nm, ε(320), presented for comparison purposes, was chosen since it is usually near the peak in weighted irradiance (Banaszak & Neale 2001) and is a wavelength of minimum variation in BWFs determined using the Rundel method. In addition, this wavelength is a good indicator of overall sensitivity. Weights within a study area varied by 2- to 3-fold, showing some significant differences in sensitivity of these assemblages.

To further characterize BWF variability, as well as obtain an overview of spectral dependence, a mean BWF (±SD) was calculated for each model. Within the samples from Stns PAL-01 to PAL-10 (Fig. 7A), the 2 samples from surface ice slurries were at the lowest end of the sensitivity and the rest of the stations were more sensitive. The assemblage at Stn WSC-04 (shown separately in Fig. 7A) had significantly higher weights from approximately 300 to 340 nm. A second group of similar BWFs is the *R* model fits for Stns WSC-01 to WSC-03 (Fig. 7B). Two other R model BWFs are shown separately: Stn PAL-11 was similar to the group mean up to 380 nm, where the values dropped off. Stn WSC-05 was not included in the mean because it was substantially less sensitive.

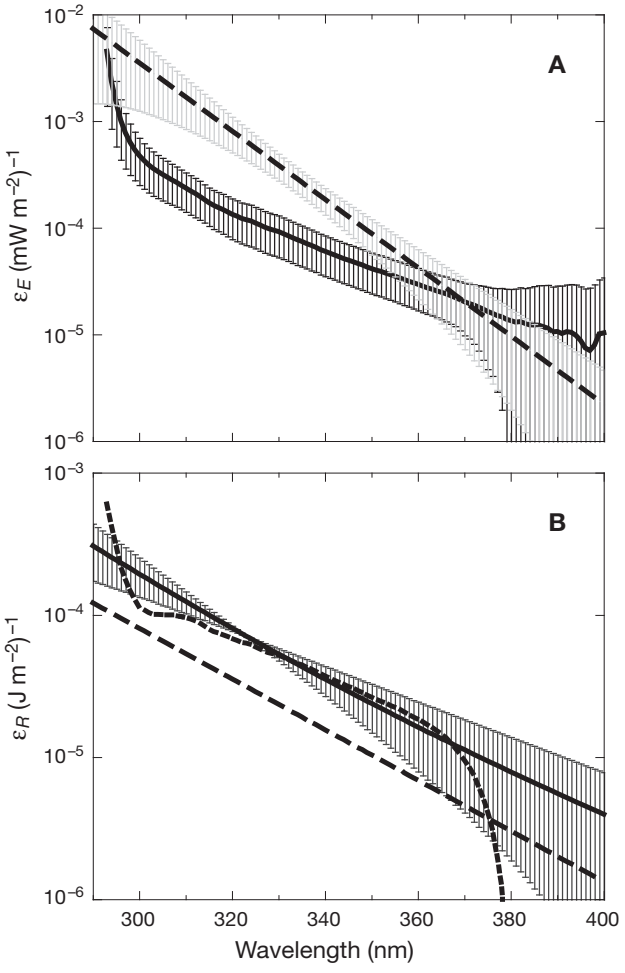

Fig. 7. (A) Biological weighting functions (BWFs) for populations using the *E* model (see 'Predicted productivity'), including the mean BWF (±SD) for Stns PAL-01 to PAL-10 (—|—) and Stn WSC-04 (– – –|– – – denoting SE). (B) BWFs using the *R* model for the following assemblages: mean of Stns WSC-01 to WSC-03 (—|—), WSC-05 (– – – – –) and PAL-11 (▪▪▪▪▪▪)

In order to compare the *E* and *R* model BWFs directly, we evaluated model predictions in the context of a 'typical' incubation exposure block of 2.5 to 3 h as used in the WSC incubations. It was observed that, for exposures of this duration and using the average repair rate estimate (discussed in the subsection 'Repair rate'), the relative rate of photosynthesis predicted by the *R* model was closely approximated by the expression $1/(1 + 0.4\ H^*_{inh})$ where H^*_{inh} is calculated from ε_R using Eq. (5) (Fig. 8A). This expression has the same form as the predicted response from the *E* model, $(1/(1 + E^*_{inh}))$. Noting that a 2.5 h exposure in J m^{-2} is 9 times the average mW m^{-2}, we established the approximate equivalence of $\varepsilon_R \cdot H \approx 0.4 \cdot 9 \cdot \varepsilon_R \cdot E = 3.6 \cdot \varepsilon_R \cdot E$, where *E* is the average irradiance during the exposure. Using this scaling on the *R* model BWFs, most of the *R* model assemblages were more sensitive overall compared to the *E* model (Fig. 8B), due primarily to the lower repair rates, although there was variation in sensitivity at both sites. The exception was at Stn WSC-05, where this assemblage, and the other PAL assemblages, were the least sensitive in the UVB and lower UVA wavelengths.

Repair rate

Transfer of samples from the high to low UVR enclosures allowed assessment of recovery from UVR inhibition. The average rates in each time block after transfer were used to fit repair rate in the *R* model (Eqs. 6 to 8). Although the fit was based on the agreement of measured and predicted average rates over 2.5 to 3 h periods, rates were calculated at 1 min intervals. This resolution shows detailed kinetics of inhibition and recovery. Two example time courses (Stns WSC-03 and PAL-11) are shown in Fig. 9. The predicted productivity of all samples decreased initially, since even the low UVR treatments were affected by some UVR and PAR inhibition. In the second time block, when H1L3 was transferred to the low UVR tank, productivity of this treatment increased progressively, while other treatments had a slow increase as UVR exposure declined (cf. Fig. 5C). When H2L2 samples were transferred (third time block), these samples also increased to near L4 productivity within 2.5 to 3 h. In general, predicted recovery was close to complete within 3 h. The predicted time courses for the other assemblages to which the *R* model was applied were similar to those in Fig. 9.

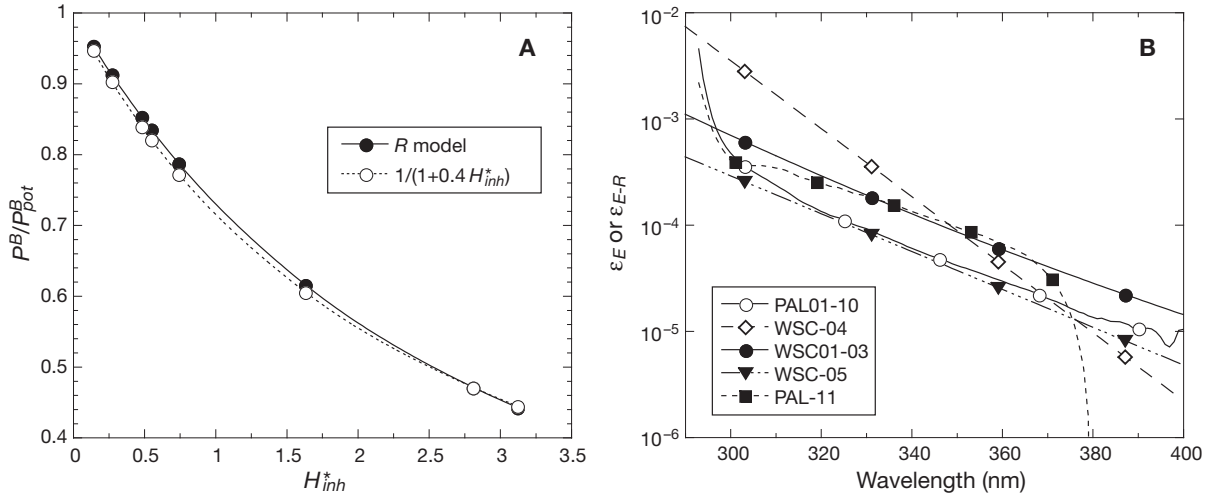

Fig. 8. (A) Average photosynthetic rate, P^B, relative to P^B_{pot} as a function of cumulative weighted exposure (H^*_{inh}) over 2.5 h. Comparison of full analytical calculation based on Eq. (8) (—●—) and an approximate calculation, $1/(1 + 0.4\ H^*_{inh})$ (---○---). The points show specific exposures that occurred in the Stn PAL-11 experiment. Calculations assume a repair rate of 0.008 min^{-1}. (B) Biological weighting functions (BWFs) for the *E* model (open symbols) and scaled *R* model (solid symbols). The scaled coefficients ($\varepsilon_{E\text{-}R}$) give an *E* model prediction equivalent to the *R* model prediction over exposures long enough to reach steady state (see 'Model input' subsection for further explanation)

Predicted productivity rates after transfer matched the measurements well (Figs. 10 & 11). We referenced H1L3 or H2L2 productivity to the rate in the L4 tank so that a ratio of 1 indicates full recovery from inhibition associated with the extra UVR in the high treatment. In all *R* model cases (Fig. 10A–D), there was only partial recovery during the first block after transfer, consistent with application of the *R* model. Near-full recovery was seen for all H1L3 assemblages by the end of the incubation. In almost all cases, H2L2 assemblages were also fully recovered, while H4 assemblages remained at a ratio of approximately 0.6. In contrast, for samples fitted with the *E* model (Fig. 10E,F), full recovery was observed immediately after transfer. Overall, predicted productivity agreed well with observed productivity for all *R* model transfer samples (Fig. 11). Almost all samples were not significantly different from a 1:1 ratio. Estimated repair rates were relatively similar between these 5 stations (Table 3) and varied from 6.84×10^{-3} to 10.98×10^{-3} min^{-1}. This translated to a recovery time scale (63% of asymptote) in the absence of UVR in the range of 1.5 to 2.4 h. Nearly complete recovery (90% of asymptote) required 3.5 to 5.6 h.

Concerning chlorophyll concentrations in transferred samples, there was no overall trend during the incubations. Most samples exhibited no trend during the incubation period, and in those that did, the differences were not significant. Populations at 3 stations (Stns WSC-02, WSC-04 and PAL-04) decreased in chlorophyll and one (Stn PAL-02) increased from the beginning to end of the incubation in H4 conditions. Only for Stn PAL-06 was L4 greater than H2L2, and H2L2 greater than H4, yet none of these were significantly different from the initial chlorophyll concentration.

The root mean square errors (RMSe), used as a measure of overall agreement between predicted and observed productivity rates for each time course, were in the range of 0.11 to 0.63 mg C (mg chl)$^{-1}$ h^{-1} for all stations (n = 12 to 16) (Table 3). The *R* model RMSe ranged from 0.11 to 0.32 mg C (mg chl)$^{-1}$ h^{-1} with an overall value of 0.26 mg C (mg chl)$^{-1}$ h^{-1}, showing the good fit of this model to the observations. The range of RMSe for the *E* model was greater, from 0.19 to 0.63 mg C (mg chl)$^{-1}$ h^{-1} with an overall value of 0.41 mg C (mg chl)$^{-1}$ h^{-1}. One source of higher RMSe for fits of both models is the occasional occurrence of increasing variability of measured rates and discrepancies between the model and the observed data during the latter samplings. These could be due to greater bottle effects after 10 to 12 h of incubation, but the specific cause is unknown and occurred despite efforts to rigorously clean and rinse bottles before use.

DISCUSSION

Previous work suggested that phytoplankton assemblages in the open waters of WSC would exhibit no or very slow recovery from UVR inhibition of photosynthesis (Neale et al. 1998a). In the kinetics portion of that study, Neale et al. (1998a) found no measurable increase in photosynthetic rate up to 4 h after removal from strong UVR exposure, which provided the pri-

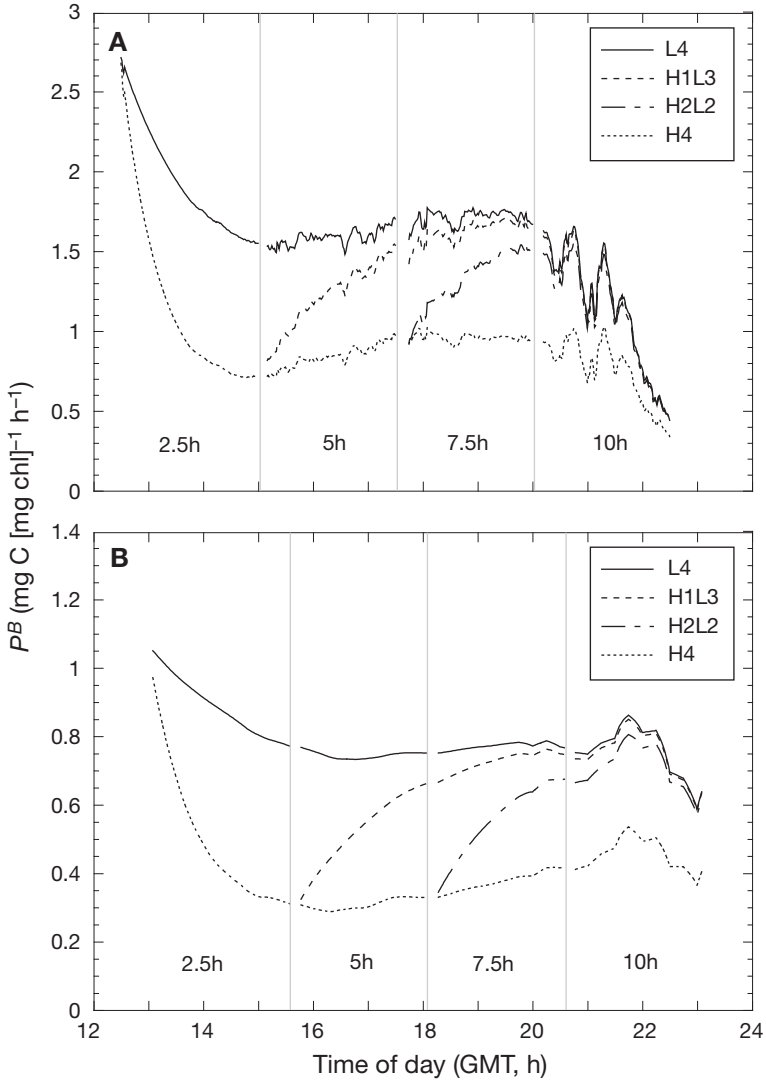

Fig. 9. Predicted time course of photosynthetic rate for all treatments in 2 experiments, Stns (A) WSC-03 and (B) PAL-11. Lines are as follows: L4 (——), H1L3 (- - - - -) and H2L2 (— - — -), H4 (· · · · · ·) (see Table 2). Model results were calculated at 1 min intervals

since some recovery can occur after transport out of the near-surface photoactive zone, compared to the previous idea that there would be no recovery regardless of light conditions (Neale et al. 1998a). We believe that a key point in the experiments of Neale et al. (1998a) was the use of short wavelength containing UVR and PAR spectrum (Xenon lamp with UVT acrylic), such that treatment exposures resulted in 100% inhibition within the first hour of exposure. As was acknowledged previously, the severity of this exposure may have suppressed repair mechanisms. In the present study, inhibition under solar UVR exposure after the first time block (2.5 to 3 h) in WSC assemblages was <30% for all stations except Stn WSC-02, which was 44% inhibited. This is significantly less inhibition over a longer exposure period and given the ability to recover, the potential for primary production is considerably greater.

The determined repair rates did not vary widely. Rates ranged from 0.007 to 0.011 min^{-1} for the 5 stations fitted with the *R* model, with near-total recovery estimated in <6 h in the absence of UVR. These rates are in the same range as previously fitted using the *R* model for photosynthesis of Lake Erie phytoplankton (Hiriart-Baer & Smith 2004, 2005) where assemblages had repair rates from 0 to 0.11 min^{-1} with a median rate of 10.2 × 10^{-3} min^{-1}, at the high end of the WSC assemblages. The recovery time in the absence of UVR varied from 1 to 6 h depending of the degree of inhibition. Although repair rates also vary for UV inhibition of macroalgal photosynthesis, slow repair rates are common for deeper growing species, especially brown (Phaeophyta) and red (Rhodophyta) macroalgae (Bischof et al. 2006). Full recovery from damage once UVR has been eliminated is generally within hours for brown algae, whereas red algae may take 24 h or longer to recover (Bischof et al. 2006, H. Miller et al. unpubl.).

mary support for use of the cumulative exposure (*H*) model. In the present study using moderate exposures to solar UVR, this was not the case. The cumulative exposure model did not fit the observed time-course of photosynthesis of WSC assemblages for exposures exceeding 2 h, apparently due to some ongoing repair. The irradiance model (Cullen et al. 1992) was also not appropriate for WSC assemblages due to the overestimation of recovery; therefore, we applied the Hiriart-Baer & Smith (2004) *R* model in which there is a low level of ongoing repair from UVR damage. This provided a significantly better fit for UVR responses of most WSC assemblages and for 1 sample from waters near Palmer Stn (Stn PAL-11). This substantially modifies our understanding of UV inhibition in the WSC

In contrast, most reports of phytoplankton response are consistent with fast kinetics and irradiance dependence. Boucher & Prézelin (1996) studied the photosynthetic response of a sample from LTER Stn B (same sample location as Stns PAL-07 and PAL-09), conducting solar time-series exposures and post-exposure measurements of photosynthesis–irradiance (*P–E*) curves. Even though daily photosynthesis was inhibited 34% by UVR exposure, daily photosynthesis estimated using *P–E* curves of the UVR-exposed samples subsequently incubated for 2 h in PAR were indistinguish-

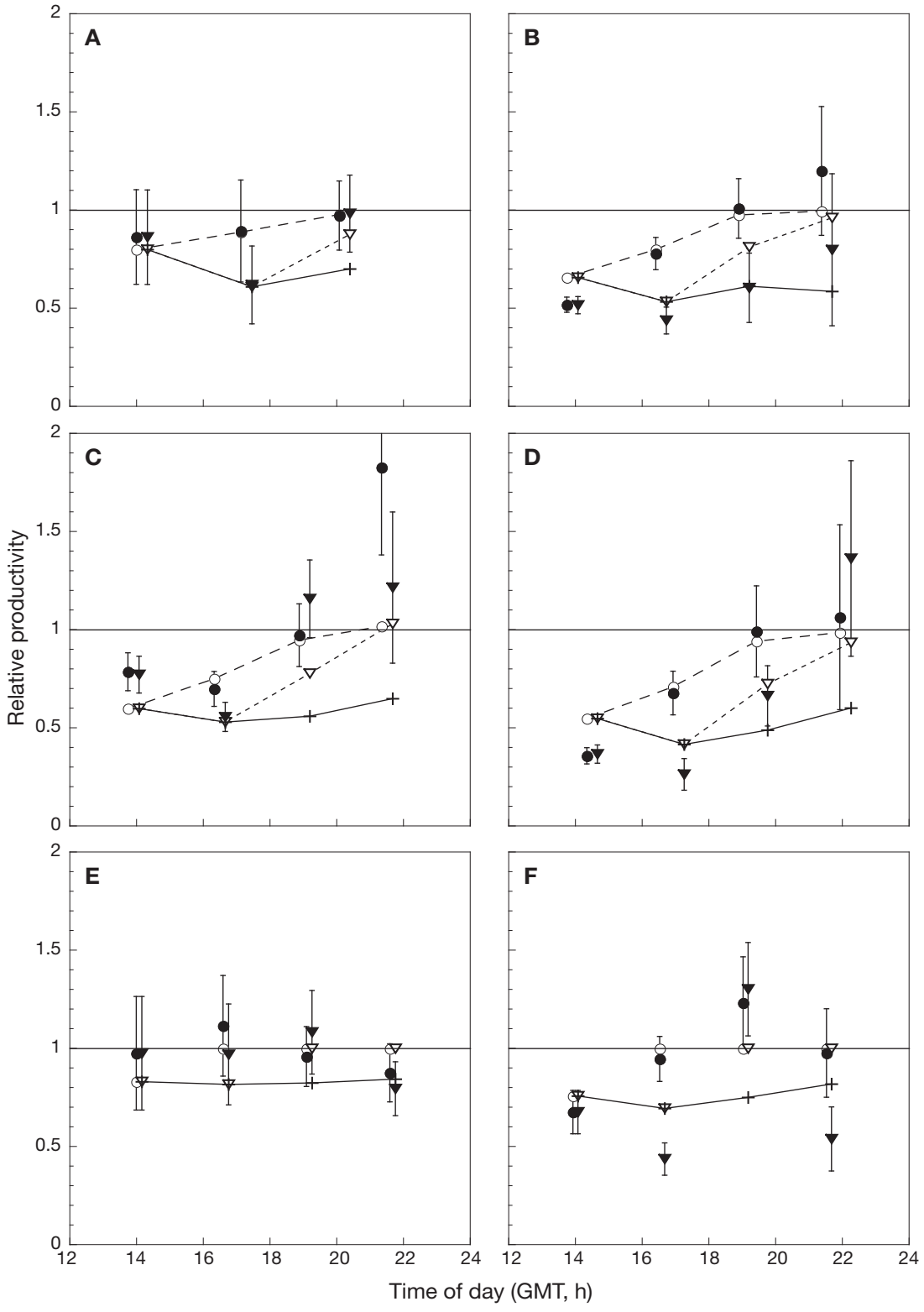

Fig. 10. Relative predicted and observed productivity for samples transferred from high UVR to low UVR during the incubation (H1L3: high exposure for 1 time block, low for 3 time blocks; H2L2: high 2 time blocks, low 2 time blocks); see Table 2. Each rate is plotted in proportion to the control (L4) rate for the same time period. Stns (A) WSC-01, (B) WSC-02, (C) WSC-03, (D) PAL-11, (E) PAL-06 and (F) PAL-09. The *R* model was applied to plots (A) to (D) and the *E* model was applied to plots (E) and (F). Observed H1L3 (●); predicted H1L3 (– – –○– – –); observed H2L2 (▼); predicted H2L2 (----▽----); predicted H4 for comparison (+). Error bars denote SE of observed relative productivity

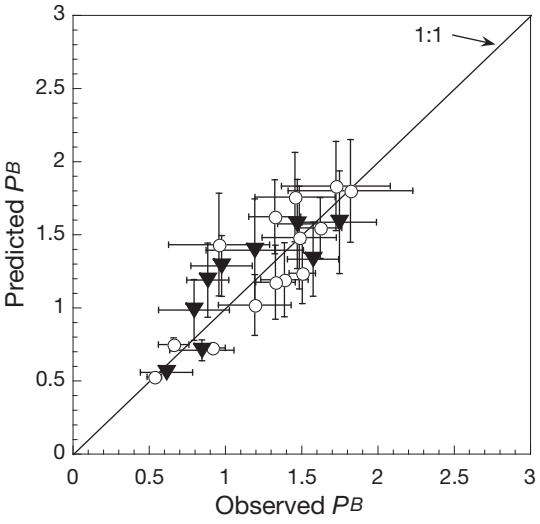

Fig. 11. Predicted versus observed photosynthesis using the *R* model (see 'Predicted productivity') for samples transferred from high to low UVR. Data include H1L3 (○) and H2L2 (▼) (see Table 2). Vertical bars are SE for model predictions. Horizontal bars are SE of measurements

able from the photosynthesis of PAR-exposed samples, which suggested that full recovery occurred in <2 h. This can be used to estimate a lower bound on recovery rate: recovery to at least 90% of photosynthesis in PAR-only samples in 2 h implies a rate of ca. 20×10^{-3} min^{-1}. This is already well above any of our *R* model estimates and actual recovery may have been faster. Therefore Boucher & Prézelin's (1996) results are consistent with our observations of generally fast recovery rates for UVR inhibition of PAL phytoplankton, for which a similar lower bound on recovery rate can be inferred.

Other reported repair rates for microalgal cultures are several-fold higher than our estimates for the WSC assemblages. Repair is so rapid in cultures that estimates require time-course measurements with a time resolution of minutes such as those obtained using PAM fluorometry. Using this approach, Shelly et al. (2003) estimated damage rates of up to 0.03 min^{-1} and ongoing repair up to 0.015 min^{-1} during UVR exposure of cultures of a temperate marine chlorophyte (*Dunaliella tertiolecta*). Once UVR was removed, maximum recovery was calculated at 0.046 min^{-1}. Litchman et al. (2002) found recovery rates of 0.09 and 0.12 min^{-1} in 2 nutrient-replete cultures of temperate dinoflagellates and fit a BWF using the *E* model. Litchman & Neale (2005) also applied the *E* model for temperate cryptophyte and diatom cultures based on unpublished PAM observations of rapid kinetics. Sobrino et al. (2005) determined a recovery rate between 0.048 and 0.086 min^{-1} in cultures of a marine picoplankton species. Overall, the ability to rapidly recover from UVR damage is present in a wide variety of algal groups and species.

For coastal Antarctic phytoplankton, Lesser et al. (1996) found that photosynthesis of high-light-acclimated assemblages from McMurdo Sound, mainly centric diatoms, was 30% lower during a 2 h incubation in full spectrum (UVT) compared to PAR-only solar irradiance, irrespective of whether it was shifted from UVT to PAR, or PAR to UVT. A similar difference was predicted using an *E* model BWF (Neale et al. 1994) applied to exposure conditions. Similarly, the majority of our coastal PAL samples were best fit using the *E* model, as was the Stn WSC-04 population, perhaps due to this latter station being located in the coastal waters off Elephant Island. Though the *E* model was a consistent predictor of productivity patterns in these samples, the overall RMSe was appreciable (0.41 mg C [mg chl]$^{-1}$ h^{-1}); however, the RMSe is not unexpectedly high given that observed rates for these experiments have an overall standard error of 0.21 mg C (mg chl)$^{-1}$ h^{-1} based on the variation between replicates.

The specific reason(s) for the consistently greater repair ability in coastal phytoplankton assemblages is unknown, though differences in species composition and average light availability could have contributed. No quantitative determinations were made of the phytoplankton community composition in the present study, but qualitative observations suggested that the species were similar to previous reports of springtime assemblages. These reports noted dominance by diatoms in the genera *Chaetoceros*, *Nitzschia* and *Thalassiosira* in the WSC (Schloss & Estrada 1994, Sigleo et al. 2000), whereas coastal waters around Elephant Island and Palmer Station are characterized by a mixture of flagellates and diatoms, such as *Corethron*, associated with the presence of ice (Schloss & Estrada 1994, Ducklow et al. 2007). All samples that were fit with the *E* model came from shallow, well-lit surface layers with PAR exceeding 22% of surface exposure (Table 3). All *R* model samples came from low-light environments except Stn PAL-11. Temperature profiles for this station were only available 2 d after the sample was taken so the light history for this sample is uncertain. Overall, these observations suggest that the generally high repair rate in coastal assemblages could be due to both the presence of species with higher repair capacity and the induction of this capacity by growth in high light. Growth in high light has been consistently associated with lower UV sensitivity (Neale et al. 1994, 1998c, Litchman & Neale 2005). Also, there are species-specific differences in repair capacity; for example, Karentz et al. (1991) reported that cultures of *Corethron cryophilum* are less sensitive than other Antarctic diatoms to UVB-induced DNA damage. Nutrient limitation can also affect repair rate (Litchman et al. 2002) but there is little evidence that this was a factor in the present study. Compared to lit-

erature values, maximum photosynthetic rates in the absence of inhibition (P_s^B) were high for the WSC (Figueiras et al. 1999) and near or somewhat below averages for the Palmer Station region (Moline et al. 1998). Furthermore, nutrient limitation (e.g. iron availability) would not be expected for springtime conditions (e.g. Ducklow et al. 2007). More study is needed of what controls repair rate of Antarctic phytoplankton in order to better understand the variation of UV inhibition kinetics in the Southern Ocean.

In addition to repair, photoprotection by screening compounds can affect overall sensitivity to UVR (e.g. Neale et al. 1998c). Of all the PAL samples, the surface ice-slurry samples had the least sensitivity to UVR (Stns PAL-06 and PAL-08). Inhibition was minimal in the case of Stn PAL-06 at roughly 2% throughout the entire incubation. In both of these samples, observed H1L3 and H2L2 were essentially equal to L4 throughout the incubation. They also had the prominent peaks in particulate absorption at 330 nm signifying the presence of mycosporine-like amino acids (MAAs; data not shown). Although MAA analysis was not performed on the 1999 samples, it was performed for the 1997 and 1998 samples (A. Banaszak unpubl. data). When present, coastal stations had both shinorine and porphyra-334, whereas 3 of the open-ocean WSC assemblages (Stns WSC-01 to WSC-03) contained low quantities of shinorine. This low concentration or complete absence of screening pigments is another factor likely contributing to the higher sensitivity of the WSC assemblages to UVR inhibition.

The finding that open-water assemblages have a slow repair capability has important implications for modeling UVR effects on primary productivity in the surface mixed layer (e.g. Arrigo et al. 2003). Observation of significant repair implies that even WSC phytoplankton can completely recover from the effects of surface exposure given sufficient time; however, as discussed by Neale et al. (2003), the overall effect of UVR on integrated water column productivity will be dependent on both the kinetics of inhibition/recovery and the rate of vertical transport. In simplified simulations of integrated productivity in mixed versus static water columns, mixing decreased the effect of UVR inhibition when predicted using the *R* model (Hiriart-Baer & Smith 2005), whereas effects increased or decreased depending on the BWF and the depth of mixing when UVR inhibition was predicted with the *H* model (Neale et al. 1998b, Hiriart-Baer & Smith 2005). The results of Neale et al. (1998b) for the WSC need to be revisited in the context of the *R* model results presented in the present study, though they expected that model predictions would not be greatly affected by recovery times on the order of several hours as was observed for most WSC stations. More importantly, realistic simulations of how productivity responds to varying solar UVR in the dynamic surface layer of the Southern Ocean are now possible by combining *R* model predictions with recently developed numerical models that accurately reproduce surface mixing processes (e.g. for Langmuir circulation, Thorpe 2004).

Acknowledgements. Many thanks go to Palmer Station and support of the staff and crew of the ARSV 'Laurence M. Gould'. We thank G. MacIntyre for sampling assistance, R. Goodrich for radiometric data analysis, W. Brinley and D. Hayes for laboratory equipment calibration support J. Lempa for assistance with model data and M. Caruso for assistance with Fig. 4. We also thank C. Sobrino, L. Franklin and 4 anonymous reviewers for their input and suggestions, which significantly improved the quality of the manuscript. This research was funded by OPP-9615342 and OPP-0127073 to P.J.N. from the National Science Foundation, Office of Polar Programs.

LITERATURE CITED

Arrigo KR, Lubin D, van Dijken GL, Holm-Hansen O, Morrow E (2003) Impact of a deep ozone hole on Southern Ocean primary production. J Geophys Res 108:C53154

Banaszak AT, Neale PJ (2001) UV sensitivity of photosynthesis in phytoplankton from an estuarine environment. Limnol Oceanogr 46:592–600

Bischof K, Gómez I, Molis M, Hanelt D and others (2006) Ultraviolet radiation shapes seaweed communities. Rev Environ Sci Biotechnol 5:141–166

Boucher NP, Prézelin BB (1996) An *in situ* biological weighting function for UV inhibition of phytoplankton carbon fixation in the Southern Ocean. Mar Ecol Prog Ser 144: 223–236

Cullen JJ, Lesser MP (1991) Inhibition of photosynthesis by ultraviolet radiation as a function of dose and dosage rate: results for a marine diatom. Mar Biol 111:183–190

Cullen JJ, Neale PJ (1997) Biological weighting functions for describing the effects of ultraviolet radiation on aquatic systems. In: Häder DP (ed) Effects of ozone depletion on aquatic ecosystems. R. G. Landes, Austin, TX, p 97–118

Cullen JJ, Neale PJ, Lesser MP (1992) Biological weighting function for the inhibition of phytoplankton photosynthesis by ultraviolet radiation. Science 258:646–650

Davidson AT (2006) Effects of ultraviolet radiation on microalgal growth, survival and production. In: Rao SDV (ed) Algal cultures, analogues of blooms and applications, Vol 2. Science Publishers, Enfield, NH, p 715–767

Ducklow H, Baker K, Martinson D, Quetin L and others (2007) Marine pelagic ecosystems: the West Antarctic Peninsula. Philos Trans R Soc Lond B 362:67–94

Figueiras F, Arbones B, Estrada M (1999) Implications of bio-optical modeling of phytoplankton photosynthesis in Antarctic waters: further evidence of no light limitation in the Bransfield Strait. Limnol Oceanogr 44:1599–1608

Heraud P, Beardall J (2000) Changes in chlorophyll fluorescence during exposure of *Dunaliella tertiolecta* to UV radiation indicate a dynamic interaction between damage and repair. Photosynth Res 63:123–134

Hiriart-Baer VP, Smith REH (2004) Models for ultraviolet radiation-dependent photoinhibition of Lake Erie phytoplankton. Limnol Oceanogr 49:202–214

Hiriart-Baer VP, Smith REH (2005) The effect of ultraviolet radiation on freshwater planktonic primary production:

the role of recovery and mixing processes. Limnol Oceanogr 50:1352–1361

Karentz D, Cleaver JE, Mitchell DL (1991) Cell survival characteristics and molecular responses of Antarctic phytoplankton to ultraviolet-B radiation. J Phycol 27:326–341

Lesser MP, Neale PJ, Cullen JJ (1996) Acclimation of Antarctic phytoplankton to ultraviolet radiation: ultraviolet-absorbing compounds and carbon fixation. Mol Mar Biol Biotechnol 5:314–325

Litchman E, Neale PJ (2005) UV effects on photosynthesis, growth and acclimation of an estuarine diatom and cryptomonad. Mar Ecol Prog Ser 300:53–62

Litchman E, Neale PJ, Banaszak AT (2002) Increased sensitivity to ultraviolet radiation in nitrogen-limited dinoflagellates: photoprotection and repair. Limnol Oceanogr 47: 86–94

McKinlay AF, Diffey BL (1987) A reference spectrum for ultraviolet induced erythema in human skin. In: Passchier WF, Bosnajakovic BFM (eds) Human exposure to ultraviolet radiation: risks and regulations. Elsevier, Amsterdam, p 83–87

Moline M, Schofield O, Boucher NP (1998) Photosynthetic parameters and empirical modelling of primary production: a case study on the Antarctic Peninsula shelf. Antarct Sci 10:45–54

Neale PJ (2000) Spectral weighting functions for quantifying the effects of ultraviolet radiation in marine ecosystems. In: de Mora SJ, Demers S, Vernet M (eds) The effects of UV radiation in marine ecosystems. Cambridge University Press, Cambridge, p 73–100

Neale PJ (2001) Modeling the effects of ultraviolet radiation on estuarine phytoplankton production: impact of variations in exposure and sensitivity to inhibition. J Photochem Photobiol B 62:1–8

Neale PJ, Fritz JJ (2001) Experimental exposure of plankton suspensions to polychromatic ultraviolet radiation for determination of spectral weighting functions. In: Slusser J, Herman JR, Gao W (eds) Ultraviolet ground- and space-based measurements, models, and effects. SPIE, International Society for Optical Engineering, San Diego, CA, p 291–296

Neale PJ, Lesser MP, Cullen JJ (1994) Effects of ultraviolet radiation on the photosynthesis of phytoplankton in the vicinity of McMurdo Station, Antarctica. In: Weiler CS, Penhale PA (eds) Ultraviolet radiation in Antarctica: measurements and biological effects. American Research Series, Vol 62. American Geophysical Union, Washington, DC, p 125–142

Neale PJ, Cullen JJ, Davis RF (1998a) Inhibition of marine photosynthesis by ultraviolet radiation: variable sensitivity of phytoplankton in the Weddell-Scotia Confluence during the austral spring. Limnol Oceanogr 43:433–448

Neale PJ, Davis RF, Cullen JJ (1998b) Interactive effects of ozone depletion and vertical mixing on photosynthesis of Antarctic phytoplankton. Nature 392:585–589

Neale PJ, Banaszak AT, Jarriel CR (1998c) Ultraviolet sunscreens in *Gymnodinium sanguineum* (Dinophyceae): mycosporine-like amino acids protect against inhibition of photosynthesis. J Phycol 34:928–938

Neale PJ, Fritz JJ, Davis RF (2001) Effects of UV on photosynthesis of Antarctic phytoplankton: models and their application to coastal and pelagic assemblages. Rev Chil Hist Nat 74:283–292

Neale PJ, Helbling EW, Zagarese HE (2003) Modulation of UVR exposure and effects by vertical mixing and advection. In: Helbling EW, Zagarese HE (eds) UV effects in aquatic organisms and ecosystems, Vol 1. Royal Society of Chemistry, Cambridge, p 107–134

Neale P, Goodrich R, Brinley W (2005) The Smithsonian-NIST-USDA-FPL network for monitoring solar ultraviolet irradiance: comparison of radiometer measurements and radiative transfer model calculations. In: Martin JW, Ryntz RA, Dickie RA (eds) Service life prediction: challenging the status quo. Federation of Societies for Coatings Technology, Blue Bell, PA, p 159–170

Parsons TR, Maita Y, Lalli CM (1984 A manual of chemical and biological methods for seawater analysis. Pergamon Press, Oxford, p 141–149

Schloss I, Estrada M (1994) Phytoplankton composition in the Weddell-Scotia Confluence area during austral spring in relation to hydrography. Polar Biol 14:77–89

Shelly K, Heraud P, Beardall J (2003) Interactive effects of PAR and UV-B radiation on PSII electron transport in the marine alga *Dunaliella tertiolecta* (Chlorophyceae). J Phycol 39:509–512

Sigleo A, Neale PJ, Spector A (2000) Phytoplankton pigments at the Weddell-Scotia confluence during the 1993 austral spring. J Plankton Res 22:1989–2006

Sobrino C, Neale PJ, Lubián LM (2005) Interaction of UV radiation and inorganic carbon supply in the inhibition of photosynthesis: spectral and temporal responses of two marine picoplankters. Photochem Photobiol 81:384–393

Thorpe SA (2004) Langmuir circulation. Annu Rev Fluid Mech 36:55–79

UNEP (United Nations Environment Programme) (2006) Scientific assessment of ozone depletion: 2006. Report no. 50. World Meteorological Organization, Nairobi

Vincent W, Neale PJ (2000) Mechanisms of UV damage to aquatic organisms. In: de Mora SJ, Demers S, Vernet M (eds) The effects of UV radiation in the marine environment. Cambridge University Press, Cambridge, p 149–176

Weiler CS, Penhale PA (eds) (1994) Ultraviolet radiation in Antarctica: measurements and biological effects, Vol 62. American Geophysical Union, Washington, DC

Initial editorial responsibility: Howard Browman, Storebø, Norway; Final editorial responsibility: Hans Heinrich Janssen, Oldendorf/Luhe, Germany

Submitted: June 4, 2007; Accepted: June 16, 2008
Proofs received from author(s): July 24, 2008